

1 **Deep electrical resistivity structure of the northern Gibraltar Arc (western Mediterranean):**
2 **evidence of lithospheric slab break-off**

3

4 Oriol Rosell *

5 Anna Martí

6 Alex Marcuello

7 Juanjo Ledo

8 Pilar Queralt

9 Eduard Roca

10 Joan Campanyà

11

12 Geomodels, Departament de Geodinàmica i Geofísica, Facultat de Geologia, Universitat de
13 Barcelona, C/Martí i Franquès s/n, 08028 Barcelona, Spain

14

15 * Corresponding author, oriolrosell@ub.edu, Phone: +34 4035913

16

17 **ABSTRACT**

18 The uncertainties about the lithospheric structure of the Gibraltar Arc have generated the
19 proposal of several contradictory models to explain its actual geodynamic setting. Here we present a
20 novel 3D model of the lithospheric electrical resistivity distribution beneath the whole Betic
21 Cordillera obtained by inverting both broad band and long period magnetotelluric data. The
22 lithosphere-asthenosphere boundary under SW Iberia is shown as being deeper than under the
23 Alboran Basin. In addition, the sensitivity tests confirm the presence of a N-S oriented low-
24 resistivity anomaly at lithospheric mantle depths East of the 4°W meridian. It coincides with an area
25 without earthquake hypocenters and low velocities, and is interpreted as asthenospheric material
26 intruded by the lateral lithospheric tearing and breaking-off of the E-directed subducting Ligurian
27 slab under the Alboran Domain. This scenario suggests that the opening of the Alboran Basin is
28 related to a westward rollback of this E-directed subducting slab.

29

30 **Introduction**

31 The convergence of the African and Iberian plates generated the Gibraltar Arc (Rif and
32 Betic Cordilleras, Fig. 1) from the Late Cretaceous (García-Dueñas *et al.*, 1992; Azañón *et al.*,
33 2002). Different geodynamic models have been proposed to explain the lithospheric structure of this
34 arc-shaped belt and the opening of the Alboran Basin based on Bouguer anomalies, heat flow,
35 earthquake locations, seismic refraction, seismic tomography, geoid anomalies and elevation data
36 (e.g. Morales *et al.*, 1997; Fernández *et al.*, 1998). Thus, the opening of the Alboran Basin has been
37 explained involving a convective removal of the thickened lithospheric root that caused uplift and
38 extension (Platt and Vissers, 1989; Platt *et al.*, 1998), a lithospheric delamination caused by
39 gravitational collapse of this thickened lithosphere (Seber *et al.*, 1996; Mezcuca and Rueda, 1997;
40 Calvert *et al.*, 2000), a westwards to southwards rollback of an oceanic slab that generated back-arc
41 extension (Royden, 1993; Lonergan and White, 1997; Gutscher *et al.*, 2002), a southeastwards
42 rollback of an oceanic slab attached to the African plate (Doglioni *et al.*, 1997, 1999a), a
43 southeastward delamination of the subcrustal lithospheric slab (Docherty and Banda, 1995) or a
44 vertical broken off piece of a previously subducting lithospheric slab (Zeck, 1996, 1997).

45 The magnetotelluric method has been proved to be a useful technique to image the
46 lithospheric resistivity structure beneath plate boundaries, providing constraints to geodynamic
47 models. Continent-continent collision areas have been the focus of many studies whether or not
48 they are active (Ledo *et al.*, 2000; Unsworth, 2010). Continent-ocean collision areas have also been
49 imaged clearly depicting the subducting oceanic slab (Wannamaker *et al.*, 1989; Brasse and Eydam,
50 2008; Brasse *et al.*, 2009). Some magnetotelluric surveys have been carried out in the central Betics
51 assuming 2D structures (Pous *et al.*, 1999; Pedrera *et al.*, 2009), but this can induce incorrect
52 interpretations in complex geological areas with 3D structures (García *et al.*, 1999; Ledo, 2005).
53 Martí *et al.* (2009a) presented a 3D resistivity model of the Central Betic Crust. To image the
54 lithospheric structure of the Betics, we extended the study area to the whole Cordillera and included

55 long period data up to 20000 s. Long period data allow for a deeper investigation depth, which is
56 crucial to characterize the lithosphere-asthenosphere boundary (LAB) and the electrical resistivity
57 of the lithospheric mantle and lower crust levels.

58 The Betic Cordillera (Fig. 2a, Fig. S1) is divided into the External Zones and the Internal
59 zones (Azañón *et al.*, 2002). The External Zones include carbonate rocks from the South Iberian
60 paleomargin as well as detritic rocks from the Flysch Trough Complex, with ages ranging from
61 Mesozoic to Cenozoic. The Internal Zones, also known as Alboran Domain, include three Paleozoic
62 to Triassic metamorphised nappe complexes. Post-orogenic Upper Miocene to Quaternary basins
63 and the Alboran basin (the backarc basin of the Gibraltar Arc) lay discordant over these units. The
64 northwesternmost mountain front of the Betic Cordillera is the only one that remains active (Ruiz-
65 Constán *et al.*, 2009). Fullea *et al.* (2010) modeled the crustal thickness as 30 km beneath the
66 External Zones and ranging beneath the Internal Zones from more than 36 km under the highest
67 mountains to 20 km near the coastline, which matches existing deep seismic profiles (García-
68 Dueñas *et al.*, 1994). The depth of the LAB under the Betic Cordillera increases from 100 km at the
69 eastern boundary to 170 km at the western one (Frizon de Lamotte *et al.*, 2004; Soto *et al.*, 2008;
70 Fullea *et al.*, 2010). None of these values were obtained from electrical resistivity models, so this is
71 the first time the lithospheric structure of the northern Gibraltar Arc has been modeled from
72 magnetotelluric data.

73

74 **Magnetotelluric data**

75 The magnetotelluric method uses natural electromagnetic fields to characterize the structure
76 of the subsurface. It is a valuable technique for imaging the lithosphere and the geometry of the
77 LAB (Jones, 1999). Its investigation depth depends on both the recording period and the resistivity
78 of the Earth.

79 The dataset we present consists of 100 magnetotelluric sites located over the Betic
80 Cordillera (Fig. 1, Fig. S1), 41 of them including long period data. The time series were processed
81 using robust algorithms (Egbert and Booker, 1986; Chave and Thomson, 2004) with remote
82 reference when possible. Apparent resistivity and phase curves obtained cover periods from 0.001 s
83 up to 20000 s in some of the sites, showing medium to high quality (Fig. S2).

84 We obtained a dimensionality map using the WALDIM code (Martí *et al.*, 2009b), based on
85 the invariant rotation parameters of the impedance tensor presented by Weaver *et al.* (2000) to
86 determine if the geoelectrical structures at different depths can be identified as 1D, 2D or 3D. The
87 results (Fig. 3) show the predominance of 3D geoelectrical behaviour for periods longer than 10 s in
88 the whole area. Thus, a 3D model is the most valid approach to properly characterize the deep
89 crustal and lithospheric electrical structure beneath the Betic Cordillera.

90

91 **Geoelectrical lithospheric structure**

92 The geoelectrical structure of the Betic lithosphere was imaged by building a 3D resistivity
93 model with 38 x 50 x 33 mesh elements. The initial model used for the inversion was a
94 homogeneous 100 ohm·m block with the only exception of the sea, which was fixed with a constant
95 value of 0.3 ohm·m according to the bathymetry of the Alboran Sea. The WSINV3DMT inversion
96 code (Siripunvaraporn *et al.*, 2005) was used for inverting the off-diagonal components of the
97 impedance tensor. The misfit between the data and the model responses has an RMS value of 5.2
98 when using only a 5% error for the impedance values. Fig. S2 shows the misfit between the data
99 and model responses at each site.

100 The resulting model (Fig. 2b-i) is characterized at upper to middle crustal levels by a
101 complex pattern of resistive and conductive zones. The shallow conductive zones are likely to be
102 related to the detrital infill of the Neogene basins such as the Guadalquivir Basin (CGU), the
103 Guadix-Baza basin (CGB) or the Granada Basin (CG). The External Zones are collectively depicted

104 up to 10.5 km thick as a body of heterogeneous resistivity values due to their complex structure and
105 variable composition of carbonate marls, mudstones and detritic rocks. To the North, South and
106 beneath these conductive domains the resistive zones correspond to the igneous and metamorphic
107 rocks of the Iberian Massif (RIM) and the metamorphic Paleozoic to Triassic rocks of the Internal
108 Zones (RIZ), which continue up to mid-low crustal levels (Fig. 2c-d). The base of these two
109 resistive bodies, located in the Moho, is not visible in the model as there is no variation in the
110 electrical resistivity between the lower crust and the upper lithospheric mantle.

111 In the Internal Zones the model shows a low-resistivity anomaly located between upper-mid
112 crustal depths of 4.5 km and 17.5 km. This conductive body (CB1) was interpreted by Martí *et al.*
113 (2009a) as basic or ultrabasic rocks containing a conducting mineral phase. It is clear from our 3D
114 model that it has no continuity towards the West and does not appear at these depths anywhere else
115 in the study area.

116 At deeper levels, the resistivity model depicts a boundary at depths between 110 km and 160
117 km that marks the transition from values of 500 – 1000 ohm·m to values as low as 10 ohm·m (Fig.
118 2h-i). These low resistivity values can correspond to asthenospheric material (Eaton *et al.*, 2009)
119 and, hence, this transition is interpreted as the boundary between the lithosphere and the
120 asthenosphere (LAB). In accordance with the model presented by Fullea *et al.* (2010), the LAB is
121 estimated to be located at 110 km under the Eastern Betics and it increases its depth toward the
122 western Betics up to 160 km.

123 Above this boundary the most remarkable, yet previously undescribed feature of the model
124 appears. This is a N-trending conductive body (CB2) located East of the 4°W meridian and
125 extending in depth from 30 km down to 62 km (Fig. 2e-f). This CB2 body, located at lithospheric
126 mantle levels, has resistivity values ranging from 5 ohm·m to 15 ohm·m and is sub-vertical, dipping
127 almost 90° West. Despite the mainly N-trend, at its northern limit it turns West 90° and continues
128 about 70 kilometers. The sensitivity tests performed to the CB2 body show that its bottom reaches

129 depths of at least 62 km, but given the loss of resolution of the magnetotelluric method beneath a
130 conductive body (Jones, 1999), its bottom can be located as far down as the asthenosphere without
131 affecting the model responses (Fig. 4).

132

133 **Geodynamic implications**

134 According to lithospheric seismic tomography studies performed in the Betic Cordillera
135 (Morales *et al.*, 1999), the location of the CB2 anomaly also compares well with a zone of low
136 seismic velocity (up to a 6% decrease). In addition, the comparison between the presented
137 resistivity model and hypocenter earthquake locations (Fig. 5) also shows a lack of hypocenters
138 inside the CB2 body. In fact, it separates 3 main domains with different seismic activity and
139 resistivity values. 1) A SW domain (D1) characterized by a resistive lithosphere which includes
140 deep hypocenters with an increasing depth towards East and South. 2) A SE less resistive domain
141 (D2) with high hypocenter density located, in this case, exclusively at upper crustal levels. 3) A N
142 domain (D3) found to be more resistive with only a few shallow hypocenters located in the Iberian
143 crust. Hence, geophysical observations point to the CB2 body to separate these main lithospheric
144 domains and to be of a less rigid nature than the surrounding materials.

145 The previously presented geodynamic models have been analyzed with the constraint of the
146 CB2 body. A convective removal or a gravitational collapse of a thickened lithosphere explain the
147 presence of asthenospheric material at lithospheric mantle levels, but the strike of the CB2 body is
148 at odds with both hypotheses, as it is clearly oriented N-S and those hypotheses would predict the
149 asthenospheric material to be E-W directed. The southeastward delamination of a subcrustal
150 lithospheric slab presented by Docherty and Banda (1995) suggests an asthenospheric upwelling
151 matching the shape of the CB2 body but, again, the NE-SW strike this hypothesis needs is not
152 compatible with the geometry of the CB2 body. Thus, the only remaining options are the ones
153 involving subduction processes.

154 To explain the N-S strike of the CB2 body, the subduction needs to be East or West-
155 directed. Although the main lithospheric subduction in the western Mediterranean is West-directed
156 (Apennine subduction, Doglioni *et al.* 1999b), an East-directed subduction has already been
157 proposed to explain the lithospheric structure of the Gibraltar Arc and the opening of the Alboran
158 Sea (e.g. Gutscher *et al.*, 2002; Krijgsman and Garcés, 2004; Bokelmann *et al.*, 2010; Díaz *et al.*,
159 2010). This hypothesis combined with the lithosphere tearing model presented by Govers and
160 Wortel (2005) allow us to interpret the CB2 body as asthenospheric material intruded into the
161 lithosphere (Fig. 6). The shape and location of this asthenospheric intrusion can be correlated with a
162 detachment of the East-directed subducting slab. A slab break-off is suitable in this setting (Govers
163 and Wortel, 2005) and explains the recent uplifting of the whole area as suggested by Zeck (1996,
164 1997). This slab detachment is limited in the North by an E-trending lithospheric tearing in which
165 asthenospheric material also intrudes at its W limit generating the 90° turn of the northern part of
166 the CB2 body. The E-trending lithospheric tearing corresponds to the boundary between the Iberian
167 plate and the eastwards subducting Ligurian oceanic lithosphere and progressively ends westwards
168 near the 5°W meridian (Fig. 6). The resulting LAB is outlined on the resistivity model in Fig. 5.
169 Geophysical evidence of lithospheric slab detachments have been previously found in other
170 subduction areas such as the Mediterranean-Carpathian region (Wortel and Spakman, 2000).

171

172 **Conclusions**

173 The deep electrical resistivity model presented in this work contributes to understanding the
174 lithospheric structure of the northern Gibraltar Arc, beneath the Betic Cordillera. The existence of a
175 low-resistivity anomaly at lithospheric mantle depths East of the 4°W meridian compares favorably
176 with the lack of earthquake hypocenter locations and a previously observed low velocity zone. The
177 geodynamic setting our model suggests is based on the magnetotelluric constraints and shows that
178 the lithospheric structure under the Betic Cordillera and the adjoining Alboran Basin are the result

179 of the westwards roll-back of an E-directed lithospheric subduction that ends towards the North in a
180 tearing sequence. This subduction resulted during its latest stages in a slab break-off phase and
181 detachment with asthenospheric material then intruding and filling the resulting gap. This model
182 partially agrees with the E-directed subduction proposed by previous works (Royden, 1993;
183 Lonergan and White, 1997; Gutscher *et al.*, 2002), but introduces the lateral lithospheric tearing and
184 the slab break-off. The outlining of the geometry of the lithosphere-asthenosphere boundary,
185 located at a range of depths from 110 km (NE) to 160 km (SW), corresponds well with the ones
186 presented by previous works, the only exception being the previously undescribed asthenospheric
187 intrusion.

188

189 **ACKNOWLEDGEMENTS**

190 The authors sincerely thank Prof. Carlo Doglioni, Dr. Rob Evans, the Associate Editor and
191 two anonymous reviewers for their useful comments on the original version of the manuscript. They
192 also wish to thank the Dublin Institute for Advanced Studies for letting us borrow the long period
193 systems used in this work and the Universidad de Granada for the Acquisition Data Units borrowed
194 in 2007. This work was supported by the Spanish Ministry of Education and EU FEDER funds
195 under the MAGBET (CGL2006-10166) and PIER-CO2 (CGL2009-07604) contracts and a FPU
196 research grant (AP2006-00232). We would like to thank Grant George Buffett for copy editing.

197

198 **REFERENCES**

199 Azañón, J.M., Galindo-Zaldívar, J., García Dueñas, V. and Jabaloy, A., 2002. Alpine Tectonics II:
200 Betic Cordillera and Balearic Islands. In: *The Geology of Spain* (W. Gibbons and T. Moreno,
201 eds), pp. 401-416. Geological Society of London, London, UK.

202 Bokelmann, G., Maufroy, E., Buontempo, L., Morales, J. and Barruol, G., 2010. Testing oceanic
203 subduction and convective removal models for the Gibraltar arc: Seismological constraints
204 from dispersion and anisotropy. *Tectonophysics*, (in press). DOI: 10.1016/j.tecto.2010.08.004.

205 Brasse, H. and Eydam, D., 2008. Electrical conductivity beneath the Bolivian Orocline and its
206 relation to subduction processes at the South American continental margin. *Journal of*
207 *Geophysical Research*, **113**, B07109. DOI: 10.1029/2007JB005142.

208 Brasse, H., Kapinos, G., Mütschard, L., Alvarado, G.E., Worzewski, T. and Jegen, M., 2009. Deep
209 electrical resistivity structure of northwestern Costa Rica. *Geophysical Research Letters*, **36**,
210 L02310. DOI: 10.1029/2008GL036397.

211 Calvert, A., Sandvol, E., Seber, D., Barazangi, M., Roecker, S., Mourabit, T., Vidal, F., Alguacil,
212 G. and Jabour, N., 2000. Geodynamic evolution of the lithosphere and upper mantle beneath
213 the Alboran region of the western Mediterranean: Constraints from travel time tomography.
214 *Journal of Geophysical Research*, **105**, 10871-10898. DOI: 10.1029/2000JB900024.

215 Chave, A.D. and Thomson, D.J., 2004. Bounded influence estimation of magnetotelluric response
216 functions. *Geophysical Journal International*, **157**, 988-1006. DOI: 10.1111/j.1365-
217 246X.2004.02203.x.

218 Díaz, J., Gallart, J., Villaseñor, A., Mancilla, F., Pazos, A., Córdoba, D., Pulgar, J.A., Ibarra, P. and
219 Harnafi, M., 2010. Mantle dynamics beneath the Gibraltar Arc (western Mediterranean) from
220 shear-wave splitting measurements on a dense seismic array. *Geophysical Research Letters*, **37**,
221 L18304. DOI: 10.1029/2010GL044201.

222 Docherty, C. and Banda, E., 1995. Evidence for the eastward migration of the Alboran Sea based on
223 regional subsidence analysis: A case for basin formation by delamination of the subcrustal
224 lithosphere? *Tectonics*, **14**, 804-818. DOI: doi:10.1029/95TC00501.

- 225 Doglioni, C., Gueguen, E., Sàbat, F. and Fernandez, M., 1997. The Western Mediterranean
226 extensional basins and the Alpine orogen. *Terra Nova*, **9**, 109-112. DOI: 10.1046/j.1365-
227 3121.1997.d01-18.x.
- 228 Doglioni, C., Fernandez, M., Gueguen, E. and Sàbat, F., 1999a. On the interference between the
229 early Apennines-Maghrebides backarc extension and the Alps-Betics orogen in the Neogene
230 Geodynamics of the Western Mediterranean. *Bollettino della Societa Geologica Italiana*, **118**,
231 75-89.
- 232 Doglioni, C., Gueguen, E., Harabaglia, P. and Mongelli, F., 1999b. On the origin of west-directed
233 subduction zones and applications to western Mediterranean. In: *The Mediterranean Basins:
234 Tertiary Extension within the Alpine Orogen* (B. Durand et al., eds). Geological Society Special
235 Publications, London. DOI: 10.1144/GSL.SP.1999.156.01.24.
- 236 Eaton, D.W., Darbyshire, F., Evans, R.L., Grütter, H., Jones, A.G. and Yuan, X., 2009. The elusive
237 lithosphere–asthenosphere boundary (LAB) beneath cratons. *Lithos*, **109**, 1-22. DOI:
238 10.1016/j.lithos.2008.05.009.
- 239 Egbert, G.D. and Booker, J.R., 1986. Robust estimation of Geomagnetic transfer functions.
240 *Geophysical Journal of the Royal Astronomical Society*, **87**, 173-194. DOI: 10.1111/j.1365-
241 246X.1986.tb04552.x.
- 242 Fernàndez, M., Marzán, I., Correia, A. and Ramalho, E., 1998. Heat flow, heat production, and
243 lithospheric thermal regime in the Iberian Peninsula. *Tectonophysics*, **291**, 29-53. DOI:
244 10.1016/S0040-1951(98)00029-8.
- 245 Frizzon de Lamotte, D., Crespo-Blanc, A., Saint-Bézar, B., Comas, M., Fernàndez, M., Zeyen, H.,
246 Ayarza, P., Robert-Charrue, C., Chalouan, A., Zizi, M., Teixell, A., Arboleya, M.L., Alvarez-
247 Lobato, F., Julivert, M. and Michard, A., 2004. Transect I: Iberian Meseta - Guadalquivir Basin
248 - Betic Cordillera - Alboran Sea – Rif - Moroccan Meseta - High Atlas - Sahara Domain. In:

249 *The TRANSMED Atlas - The Mediterranean Region from Crust to Mantle* (W. Cavazza et al.,
250 eds). Springer, Berlin-Heidelberg.

251 Fullea, J., Fernández, M., Afonso, J.C., Vergés, J. and Zeyen, H., 2010. The structure and evolution
252 of the lithosphere–asthenosphere boundary beneath the Atlantic–Mediterranean Transition
253 Region. *Lithos*, **120**, 74-95. DOI: 10.1016/j.lithos.2010.03.003.

254 García, X., Ledo, J. and Queralt, P., 1999. 2D inversion of 3D magnetotelluric data: The Kayabe
255 dataset. *Earth, Planets and Space*, **51**, 1135-1143.

256 García-Dueñas, V., Balanyá, J.C. and Martínez-Martínez, J., 1992. Miocene extensional detachment
257 in the outcropping basement of the northern Alboran basin (Betics) and their tectonic
258 implications. *Geo-Marine Letters*, **12**, 88-95. DOI: 10.1007/BF02084917.

259 García-Dueñas, V., Banda, E., Torné, M. and Córdoba, D., 1994. A deep seismic-reflection survey
260 across the Betic Chain (southern Spain): first results. *Tectonophysics*, **232**, 77-89. DOI:
261 10.1016/0040-1951(94)90077-9.

262 Govers R. and Wortel, M.J.R., 2005. Lithosphere tearing at STEP faults: Response to edges of
263 subduction zones. *Earth and Planetary Science Letters*, **236**, 505-523. DOI:
264 10.1016/j.epsl.2005.03.022.

265 Gutscher, M.A., Malod, J., Rehault, J.P., Contrucci, I., Klingelhoefer, F., Mendes-Victor, L. and
266 Spakman, W., 2002. Evidence for active subduction beneath Gibraltar. *Geology*, **30**, 1071-
267 1074. DOI: 10.1130/0091-7613(2002)030<1071:EFASBG>2.0.CO;2.

268 Jones, A.G., 1999. Imaging the continental upper mantle using electromagnetic methods. *Lithos*, **48**,
269 57-80. DOI: 10.1016/S0024-4937(99)00022-5.

270 Krijgsman, W. and Garcés, M., 2004. Palaeomagnetic constraints on the geodynamic evolution of
271 the Gibraltar Arc. *Terra Nova*, **16**, 281-287. DOI: 10.1111/j.1365-3121.2004.00564.x.

272 Ledo, J., Ayala, C., Pous, J., Queralt, P., Marcuello, A. and Muñoz, J.A., 2000. New geophysical
273 constraints on the deep structure of the Pyrenees. *Geophysical Research Letters*, **27**, 1037-
274 1040. DOI: 10.1029/1999GL011005.

275 Ledo, J., 2005. 2-D versus 3-D magnetotelluric data interpretation. *Surveys in Geophysics*, **26**, 511-
276 543. DOI: 10.1007/s10712-005-1757-8.

277 Lonergan, L. and White, N., 1997. Origin of the Betic-Rif mountain belt. *Tectonics*, **16**, 504-522.
278 DOI: 10.1029/96TC03937.

279 Martí, A., Queralt, P., Roca, E., Ledo, J. and Galindo-Zaldívar, J., 2009a. Geodynamic implications
280 for the formation of the Betic-Rif orogen from magnetotelluric studies. *Journal of Geophysical*
281 *Research*, **114**, B01103. DOI: 10.1029/2007JB005564.

282 Martí, A., Queralt, P. and Ledo, J., 2009b. WALDIM: A code for the dimensionality analysis of
283 magnetotelluric data using the rotational invariants of the magnetotelluric tensor. *Computers &*
284 *Geosciences*, **35**, 2295-2303. DOI:10.1016/j.cageo.2009.03.004.

285 Mezcuca, J. and Rueda, J., 1997. Seismological evidence for a delamination process in the
286 lithosphere under the Alboran Sea. *Geophysical Journal International*, **129**, F1-F8. DOI:
287 10.1111/j.1365-246X.1997.tb00934.x.

288 Morales, J., Serrano, I., Vidal, F. and Torcal, F., 1997. The depth of the earthquake activity in the
289 Central Betics (Southern Spain). *Geophysical Research Letters*, **24**, 3289-3292. DOI:
290 10.1029/97GL03306.

291 Morales, J., Serrano, I., Jabaloy, A., Galindo-Zaldívar, J., Zhao, D., Torcal, F., Vidal, F. and
292 González-Lodeiro, F., 1999. Active continental subduction beneath the Betic Cordillera and the
293 Alborán Sea. *Geology*, **27**, 735-738, DOI: 10.1130/0091-
294 7613(1999)027<0735:ACSBTB>2.3.CO;2.

295 Pedrera, A., Galindo-Zaldívar, J., Ruíz-Constán, A., Duque, C., Marín-Lechado, C. and Serrano I.,
296 2009. Recent large fold nucleation in the upper crust: Insight from gravity, magnetic,

297 magnetotelluric and seismicity data (Sierra de los Filabres-Sierra de las Estancias, Internal
298 Zones, Betic Cordillera). *Tectonophysics*, **463**, 145-160. DOI: 10.1016/j.tecto.2008.09.037.

299 Platt, J.P. and Vissers, R.L.M., 1989. Extensional collapse of thickened continental lithosphere: A
300 working hypothesis for the Alboran Sea and Gibraltar Arc. *Geology*, **17**, 540-543. DOI:
301 10.1130/0091-7613(1989)017<0540:ECOTCL>2.3.CO;2.

302 Platt, J.P., Soto, J.I., Whitehouse, M.J., Hurford, A.J. and Kelley, S.P., 1998. Thermal evolution,
303 rate of exhumation, and tectonic significance of metamorphic rocks from the floor of the
304 Alboran extensional basin, western Mediterranean. *Tectonics*, **17**, 671-689. DOI:
305 10.1029/98TC02204.

306 Pous, J., Queralt, P., Ledo, J. and Roca, E., 1999. A high electrical conductive layer zone at lower
307 crustal depth beneath the Betic Chain (Spain). *Earth and Planetary Science Letters*, **167**, 35-45.
308 DOI: 10.1016/S0012-821X(99)00011-4.

309 Royden, L.H., 1993. Evolution of retreating subduction boundaries formed during continental
310 collision. *Tectonics*, **12**, 629-638. DOI: 10.1029/92TC02641.

311 Ruiz-Constán, A., Stich, D., Galindo-Zaldívar, J. and Morales, J., 2009. Is the northwestern Betic
312 Cordillera mountain front active in the context of the convergent Eurasia–Africa plate
313 boundary? *Terra Nova*, **21**, 352-359. DOI: 10.1111/j.1365-3121.2009.00886.x.

314 Seber, D., Baranzagi, M., Ibenbrahim, A. and Demnati, A., 1996. Geophysical evidence for
315 lithospheric delamination beneath the Alboran Sea and Rif-Betic mountains. *Nature*, **379**, 785-
316 790. DOI: 10.1038/379785a0.

317 Siripunvaraporn, W., Egbert, G., Lenbury, Y. and Uyeshima, M., 2005. Three-Dimensional
318 Magnetotelluric: Data Space Method. *Physics of the Earth and Planetary Interiors*, **150**, 3-14.
319 DOI: 10.1016/j.pepi.2004.08.023.

- 320 Soto, J.I., Fernández-Ibáñez, F., Fernández, M. and García-Casco, A., 2008. Thermal structure of
321 the crust in the Gibraltar Arc: Influence on active tectonics in the Western Mediterranean.
322 *Geochemistry, Geophysics and Geosystems*, **9**, Q10011. DOI: 10.1029/2008GC002061.
- 323 Unsworth, M., 2010. Magnetotelluric Studies of Active Continent-Continent Collisions. *Surveys in*
324 *Geophysics*, **31**, 137-161. DOI: 10.1007/s10712-009-9086-y.
- 325 Wannamaker, P., Booker, J., Jones, A., Chave, A., Filloux, J., Waff, H. and Law, K., 1989.
326 Resistivity Cross Section Through the Juan de Fuca Subduction System and Its Tectonic
327 Implications. *Journal of Geophysical Research*, **94**, B10. DOI: 10.1029/JB094iB10p14127.
- 328 Weaver, J.T., Agarwal, A.K. and Lilley, F.E.M., 2000. Characterization of the magnetotelluric
329 tensor in terms of its invariants. *Geophysical Journal International*, **141**, 321-336. DOI:
330 10.1046/j.1365-246x.2000.00089.x.
- 331 Wortel, M.J.R. and Spakman, W., 2000. Subduction and Slab Detachment in the Mediterranean-
332 Carpathian Region. *Science*, **290**, 1910-1917. DOI: 10.1126/science.290.5498.1910
- 333 Zeck, H.P., 1996. Betic-Rif orogeny: Subduction of Mesozoic Tethys lithosphere under westward
334 drifting Iberia, slab detachment shortly before 22 Ma, and subsequent uplift and extensional
335 tectonics. *Tectonophysics*, **254**, 1-16. DOI: 10.1016/0040-1951(95)00206-5.
- 336 Zeck, H.P., 1997. Mantle peridotites outlining the Gibraltar Arc: Centrifugal extensional allochthons
337 derived from the earlier Alpine, westward subducted nappe pile. *Tectonophysics*, **281**, 195-207.
338 DOI: 10.1016/S0040-1951(97)00067-X.

339

340 **FIGURE CAPTIONS**

341 Figure 1. Regional tectonic scheme of the western Mediterranean showing the main tectonic units.
342 The dashed line frames the study area. Black dots indicate the location of the magnetotelluric sites.

343

344 Figure 2. (a) Simplified geological map of the study area with distinguished main tectonic units in
345 the Betic Cordillera. IM-Iberian Massif (dark grey); IZ-Internal Zones (orange); EZ-External Zones
346 (light grey); NB-Neogene Basins (white). (b-i): Top view slices selected from the 3D resistivity
347 model with the main resistive and conductive bodies identified. RIM-Resistive Iberian Massif, RIZ-
348 Resistive Internal Zones, CGU-Conductive Guadalquivir Basin, CG-Conductive Granada Basin,
349 CGB-Conductive Guadix-Baza Basin, CB1-Conductive Body 1, CB2-Conductive Body 2. Black
350 dots show the locations of the magnetotelluric sites. A-A', B-B' and C-C' on each slice show the
351 location of the vertical slices in Fig. 5.

352
353 Figure 3. Dimensionality analysis results from the magnetotelluric data at six period bands. Black
354 dots indicate lack of information at the corresponding site and period band.

355
356 Figure 4. Results from the sensitivity tests performed to the CB2 body, comparing the RMS value
357 obtained for the whole dataset when placing its base at different depths.

358
359 Figure 5. (a) Geological map of the Betics with the location of the magnetotelluric sites (black dots)
360 and the slices. A-A', B-B' and C-C' are side-view slices of the 3D resistivity model crossing the
361 CB2 body including the hypocenter locations (white dots) within 8 km from each profile recorded
362 since 1900. Dashed black line shows the lithosphere-asthenosphere boundary inferred from the
363 resistivity distribution. D1, D2 and D3 are the main tectonic domains described in the text.

364
365 Figure 6. (a-b) Geodynamic 3D scheme and cross-section of the inferred lithospheric structure
366 under the Betics and northern Alboran Sea. IC-Iberian Crust; AC-Alboran Crust (Internal Betics
367 and Alboran Sea); LC-Ligurian Crust; ILM-Iberian Lithospheric Mantle; ALM-Alboran
368 Lithospheric Mantle; LLM-Ligurian Lithospheric Mantle. AS-Asthenosphere. Dashed black line

369 shows the coast-line. (c) Inferred lithospheric structure superposed to the corresponding resistivity
370 model slice A-A'.

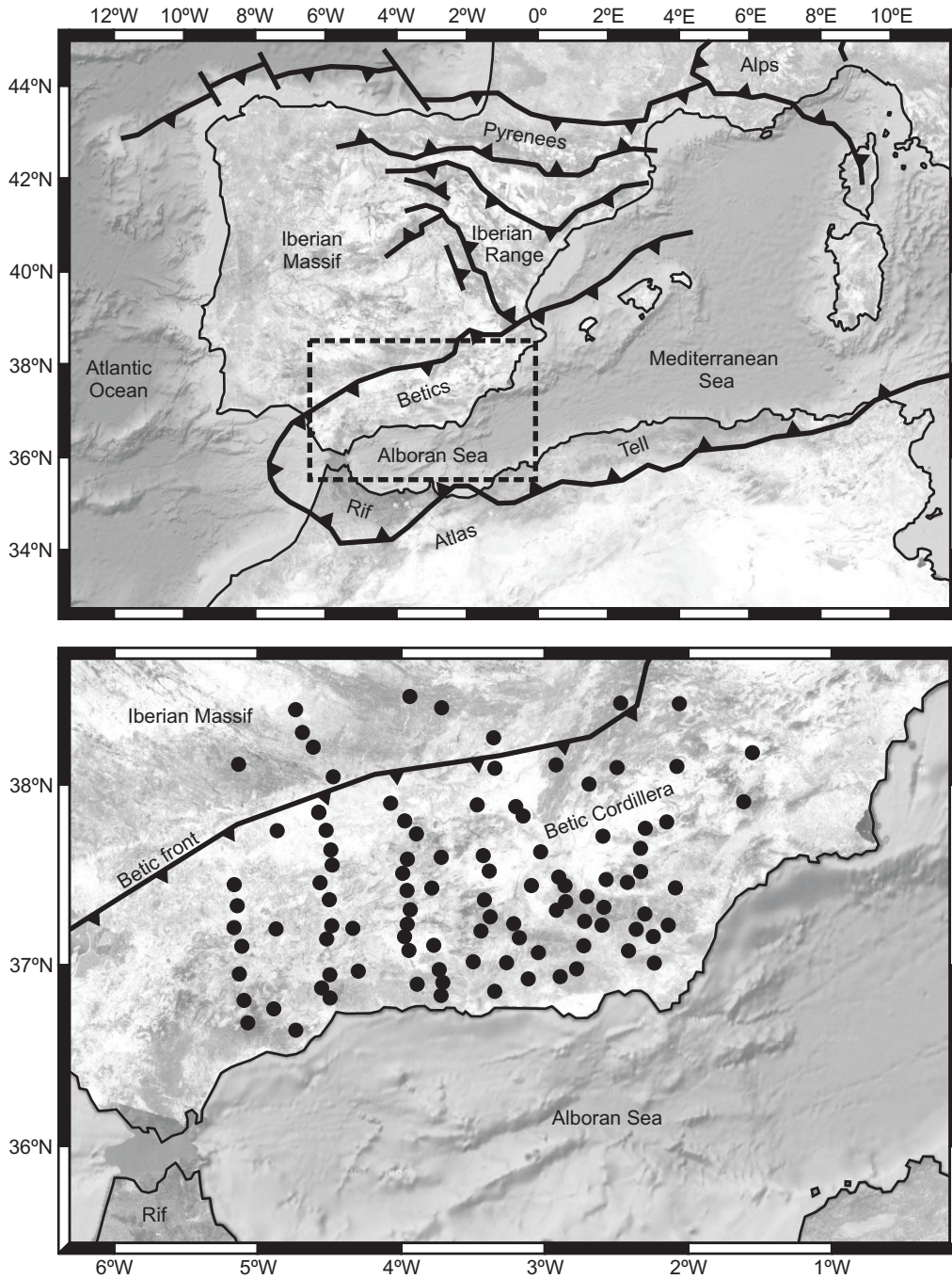


Figure 1 Rosell et al. (2010)

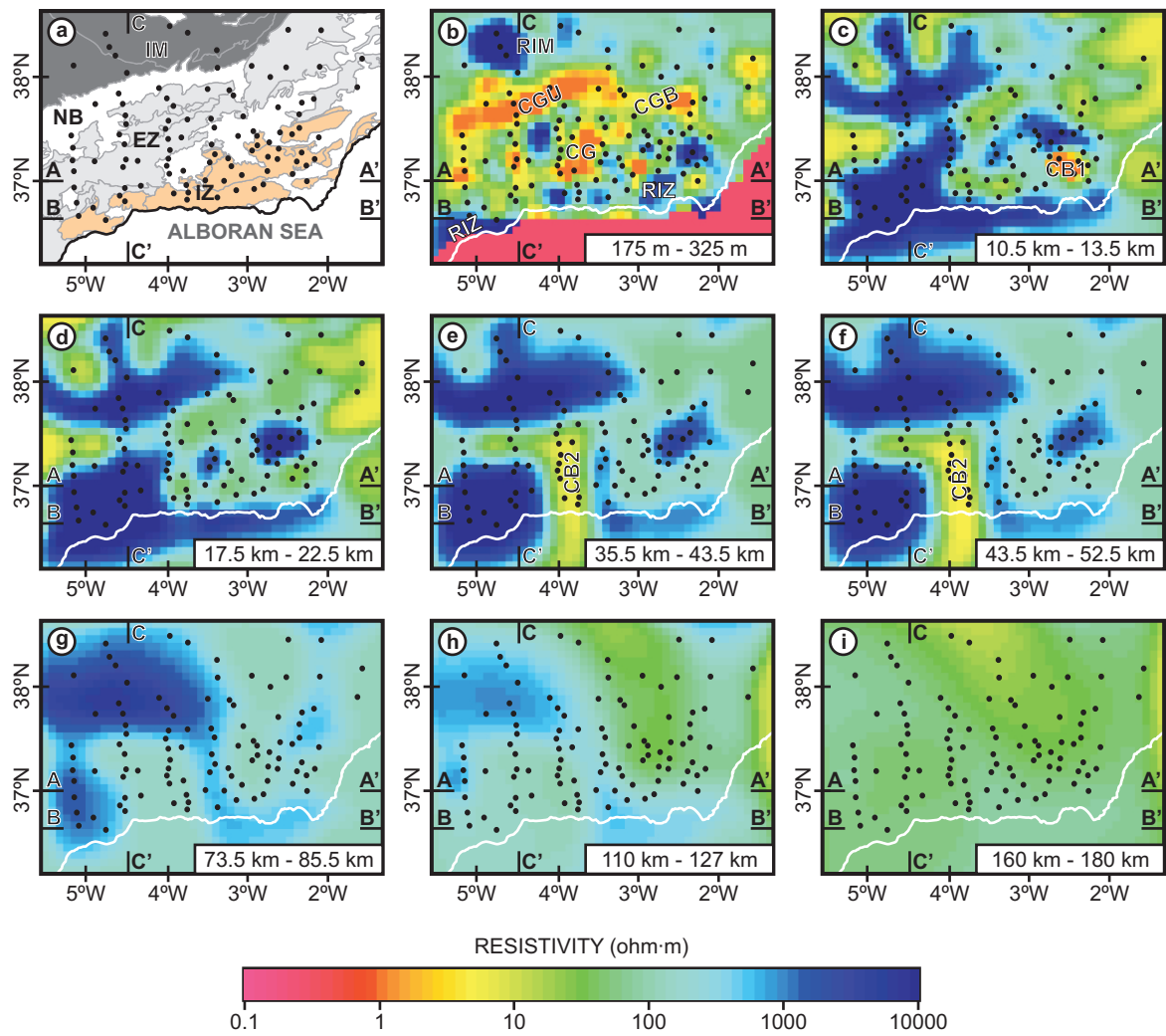


Figure 2 Rosell et al. (2010)

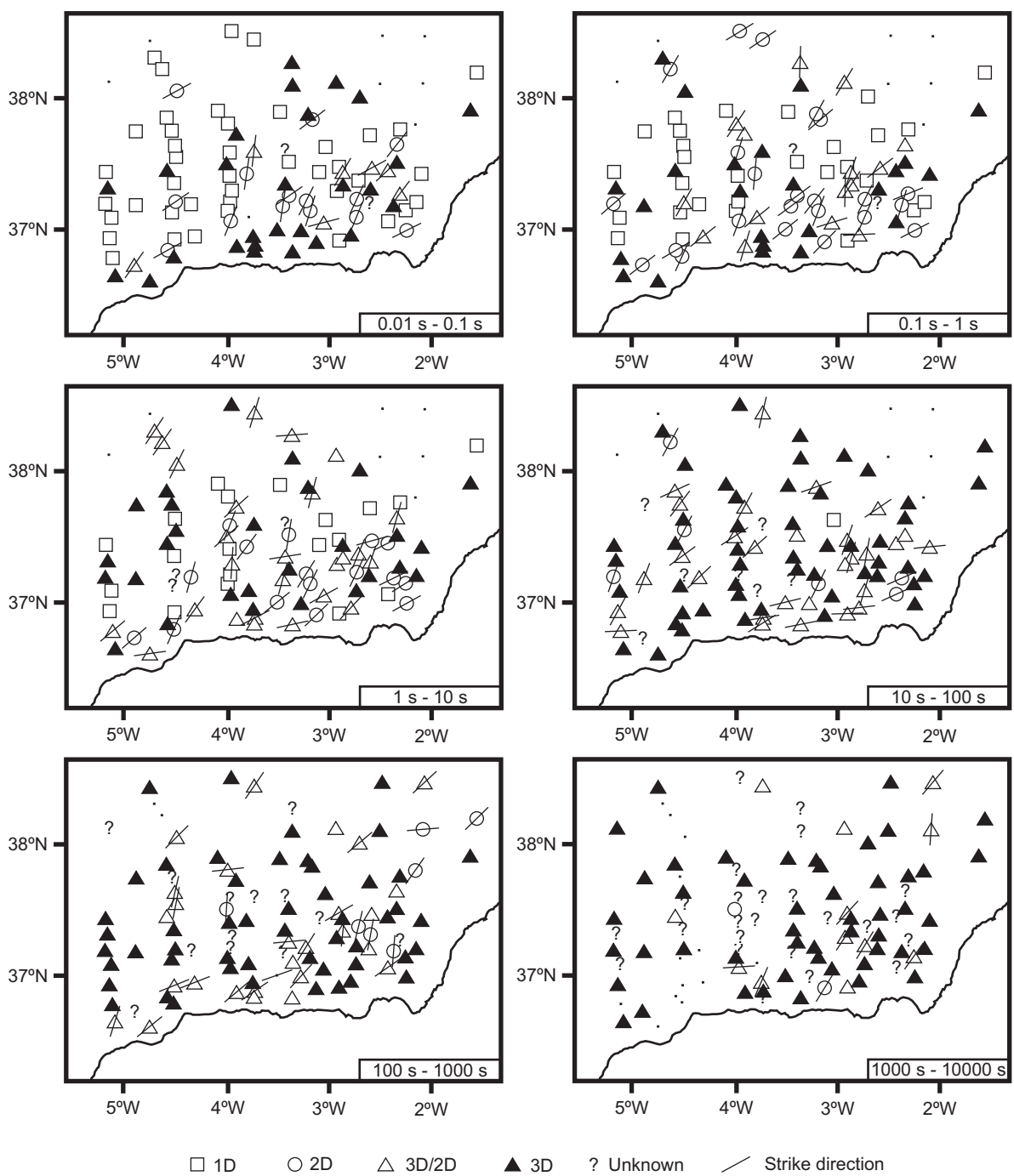


Figure 3 Rosell et al. (2010)

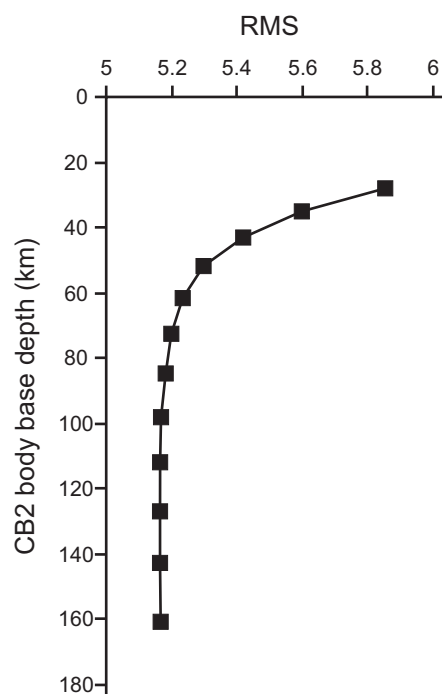


Figure 4 Rosell et al. (2010)

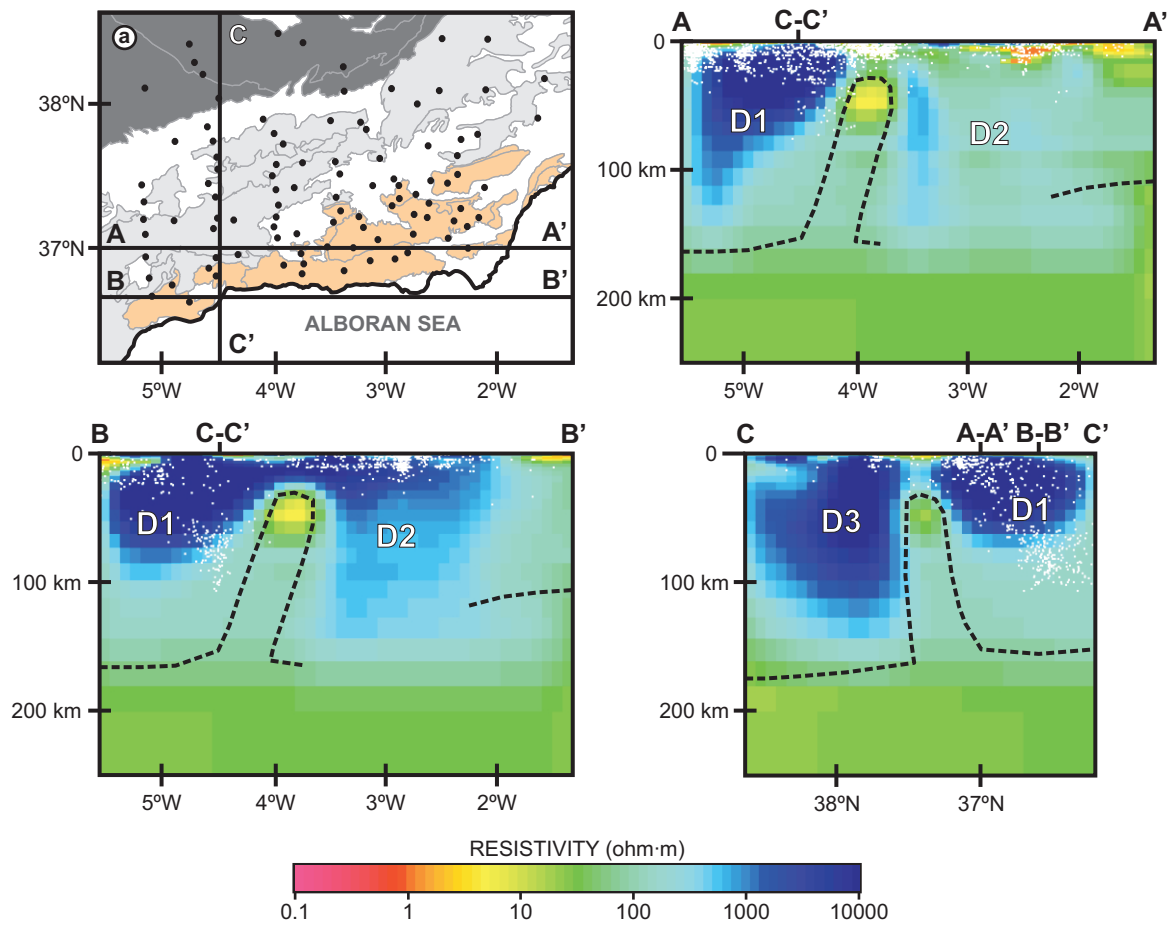


Figure 5 Rosell et al. (2010)

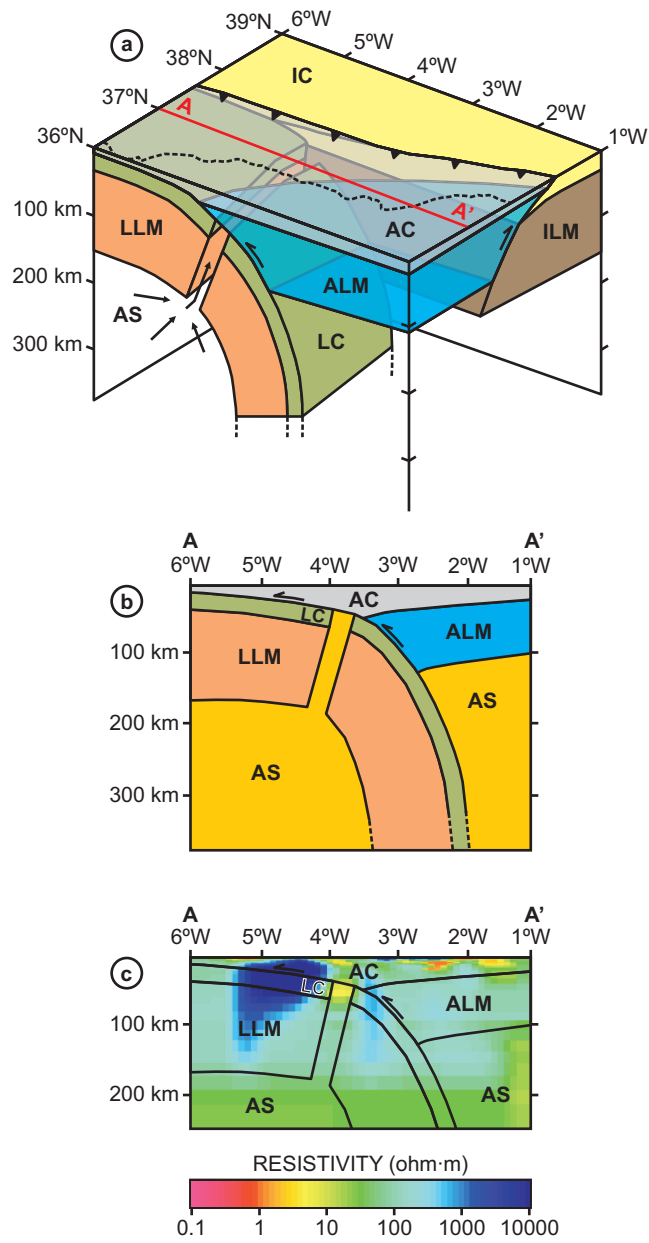


Figure 6 Rosell et al. (2010)